Editors' Suggestion

Energy deposition studies for the LHCb insertion region of the CERN Large Hadron Collider

Alessia Ciccotelli*

Department of Physics and Astronomy, School of Natural Sciences, The University of Manchester and the Cockcroft Institute, Oxford Road, Manchester M13 9PL, United Kingdom and CERN, CH 1211 Geneva 23, Switzerland

Robert B. Appleby

Department of Physics and Astronomy, School of Natural Sciences, The University of Manchester and the Cockcroft Institute, Oxford Road, Manchester M13 9PL, United Kingdom

Francesco Cerutti, Kacper Bilko, Luigi Salvatore Esposito, Ruben Garcia Alia, Anton Lechner, and Andrea Tsinganis†

CERN, CH 1211 Geneva 23, Switzerland

(Received 10 June 2022; revised 8 February 2023; accepted 18 April 2023; published 15 June 2023)

The LHCb (Large Hadron Collider beauty) experiment at CERN LHC aims at achieving a significantly higher luminosity than originally planned by means of two major upgrades: the Upgrade I that took place during the Long Shutdown 2 (LS2) and the Upgrade II proposed for LS4. Such an increase in instantaneous and integrated luminosity with respect to the design values requires to reassess the radiation exposure of LHC magnets, cryogenics, and electronic equipment placed in the insertion region 8 (IR8) around LHCb. Monte Carlo simulations are a powerful tool to understand and predict the interaction between particle showers and accelerator elements, especially in case of future scenarios. For this purpose, their validation through the comparison with available measurements is a relevant step. A detailed IR8 model, including the LHCb detector, has been implemented with the FLUKA code. The objective of this study is to evaluate radiation levels due to proton-proton collisions and benchmark the predicted dose values against beam loss monitor measurements performed in 2018. Finally, we comment on the upcoming LHC run (Run 3, from 2022 to 2025), featuring a first luminosity jump in LHCb.

DOI: 10.1103/PhysRevAccelBeams.26.061002

I. INTRODUCTION

During Run 2 (2015–2018), the Large Hadron Collider (LHC) at CERN collided 6.5 TeV proton beams at a center of mass energy $\sqrt{s} = 13$ TeV, achieving more than twice its design instantaneous luminosity in the ATLAS and CMS detectors [1]. The instantaneous luminosity $\mathcal{L}$ is defined as the proportionality factor between the number of events per second $\frac{dN}{dt}$ and their microscopic cross section σ, and its unit is therefore $\mathrm{cm}^{-2}\,\mathrm{s}^{-1}$ [2], as in Eq. (1):

$$\frac{dN}{dt} = \mathcal{L}\sigma. \tag{1}$$

The integration over the time of the instantaneous luminosity is an equally relevant quantity because it is directly linked to the number of collisions useful for the high-energy physics program. The unit of integrated luminosity $\mathcal{L}_{\mathrm{int}}$ used in this paper is the inverse femtobarn fb^{-1}.

$$\mathcal{L}_{\mathrm{int}} = \int_0^T \mathcal{L}(t')dt'. \tag{2}$$

ATLAS [3] and CMS [4] are the two general-purpose experiments, designed to cover many possible physics searches, from precision measurements of the Higgs boson to new physics beyond the Standard model. They have enormous experimental apparatus providing a 4π coverage around the beam interaction point. They require the highest possible luminosity for searches for new particles and rare processes or investigations on properties of already known particles with the best possible precision.

On the other hand, LHCb [5] is dedicated to high precision measurements of rare decays and in general to the study of particles containing the beauty quark (b quark) to investigate differences between matter and antimatter.

*alessia.ciccotelli@cern.ch

†Present address: European Commission, Joint Research Centre (JRC), B-2440 Geel, Belgium.

TABLE I. Overview of operational conditions for proton-proton collisions [12–17].

Period		Run 2 2015–2018	Run 3 2022–2025	Run 4 2029–2032	Post-LS4 2035
Beam energy		6.5 TeV	6.8 TeV	6.8–7 TeV	7 TeV
LHCb	$\mathcal{L}_{\text{int}}$	6.6 fb^{-1} [a]	25–30 fb^{-1}	25–30 fb^{-1}	400 fb^{-1} by the end of HL-LHC [c]
	$\mathcal{L}$	4×10^{32} $\text{cm}^{-2}\,\text{s}^{-1}$	2×10^{33} $\text{cm}^{-2}\,\text{s}^{-1}$	2×10^{33} $\text{cm}^{-2}\,\text{s}^{-1}$	1.5×10^{34} $\text{cm}^{-2}\,\text{s}^{-1}$ [c]
GPDs [b]	$\mathcal{L}_{\text{int}}$	160 fb^{-1}	250–300 fb^{-1}	560 fb^{-1}	4000 fb^{-1} by the end of HL-LHC
	$\mathcal{L}$	2×10^{34} $\text{cm}^{-2}\,\text{s}^{-1}$	2×10^{34} $\text{cm}^{-2}\,\text{s}^{-1}$	5×10^{34} $\text{cm}^{-2}\,\text{s}^{-1}$	5–7.5 $\times 10^{34}$ $\text{cm}^{-2}\,\text{s}^{-1}$

[a]The integrated luminosity previously delivered during Run 1 is 3.4 fb^{-1}.
[b]General purpose detectors installed at the LHC: ATLAS and CMS.
[c]In case of the Upgrade II of LHCb.

The LHCb experiment, located in the insertion region 8 (IR8), was designed to work at a lower luminosity than ATLAS and CMS, as shown in Table I, implying a lower need for protection of the LHC elements from the collision debris and therefore a different layout around the interaction point (IP). During the Long Shutdown 2 (LS2, from 2019 to mid-2022), the LHCb detector has been upgraded in order to increase its statistical precision, undergoing its so-called Upgrade I [6]. Previously, LHCb obtained a set of impressive physics results such as the first observation of CP violation in B_s^0 and charged B meson decays. Even if no significant signs of new physics have been found yet, the data analysis showed the emergence of a disagreement with the Standard Model predictions in the measurement of rare B decays at the level of 2–3 sigma [7–9]. The increased luminosity of Run 3 (2022–2025) and the following Run 4, as reported in Table I, will allow LHCb to reduce the uncertainty of these measurements and possibly unveil new phenomena [10]. The Upgrade I of LHCb mainly concerns the tracking system and the electronics of most subdetectors due to the conversion into a full software trigger system and a trigger-less readout system, *de facto* removing the limitation from hardware trigger technology. As a result of Upgrade I, the LHCb experiment expects to sustain a peak luminosity of 2×10^{33} $\text{cm}^{-2}\,\text{s}^{-1}$ which is around 5 times higher than the maximum value reached during the Run 2 proton operation. Moreover, the Upgrade II [11] envisaged for the LS4, profiting from the use of new detector technologies, aims to operate at 1.5×10^{34} $\text{cm}^{-2}\,\text{s}^{-1}$ and a center of mass energy $\sqrt{s} = 14$ TeV and to reach an integrated luminosity of 400 fb^{-1} by the end of the High Luminosity LHC (HL-LHC) era.

The challenges implied by this substantial increase in luminosity concern not only the detector (which is outside the scope of this paper, being the subject of extensive studies by the LHCb Collaboration [6,18]), but also the LHC machine, exposed to a much higher collision debris power. In particular, the consequences of its impact on accelerator elements, surrounding devices and environment have to be anticipated and be under control. Because of the complexity of the LHC layout and infrastructure, radiation levels are calculated by means of Monte Carlo simulations. We used the FLUKA code [19–21], version 4-2, which is a multipurpose Monte Carlo code widely employed to describe particle transport and interactions in many applications and extensively tested at CERN and in other laboratories for such complex geometries and high energy physics problems. In this regard, several authors have obtained a remarkable agreement comparing FLUKA calculation results with experimental data as well as results of independent modeling [22–25]. Thanks to the proven reliability of this technique, the design of new machines and pieces of equipment can be driven by energy deposition predictions that define operation challenges and machine and detector component lifetime [26–29].

In particular, depending on the level and distribution of the power density absorbed by the LHC magnet coils as a consequence of the radiation impact, superconducting cables may warm above a critical temperature and so lose their ability to conduct electricity without resistance. Such a sudden and violent transition to the normal conducting state, implying the loss of the required magnetic field and the beam dump, is referred to as *quench*. Although the superconducting state can later be restored and the beam reinjected, the collider operation at a given luminosity is not possible if the respective collision debris leads to regularly surpass the quench limit. Moreover, for both superconducting and normal conducting magnets, the coil material, especially the insulator, progressively deteriorates. This damage is a function of the accumulated radiation dose, which thereby limits the equipment's lifetime. In this paper, we evaluate these relevant quantities in view of the LHCb luminosity increase targeted in the upcoming LHC Run 3 (see Table I) in order to systematically confirm the upgrade sustainability on the accelerator side and anticipate possible issues.

There has been a variety of FLUKA models of IR8 developed at CERN in the last ten years for different types of calculations. In 2010, the first FLUKA study evaluated dose and fluence levels in the experimental cavern for

Run 1 and Run 2 [30] to assess radiation induced effects on electronics. In addition, FLUKA simulations were used to evaluate the machine induced background to the LHCb experiment [31]. Other investigations on the impact of the collision debris on the machine elements were carried out for Upgrade I scenarios based on the detector model and the optics corresponding to Run 2 [32,33]. From the perspective of the LHCb collaboration, radiation levels in the immediate surroundings of the detector were calculated and analyzed with FLUKA [18] during Run 2. No simulation studies have been carried out on the entire cavern for the Run 3 configuration, especially where LHC electronics racks are placed. Furthermore, while a comparison of the predicted dose values with beam loss monitor (BLM) measurements on the right-side magnets was already published for Run 1 [22], no benchmarking was performed yet for Run 2 at a center of mass energy of 13 TeV, nor for the opposite (asymmetric) side. Therefore, the aforementioned models have been now merged and improved for the present study, combining a more accurate implementation of the LHCb detector with an extensive description of the LHC infrastructure and beamline, and this way producing an updated framework for future investigations. These will be especially devoted to the implications of Upgrade II, after the preliminary analysis [32,34] that identified the key points toward which dedicated simulations should be directed, building on the results described in this paper. Our region of interest is presented in Sec. II. In Sec. III, a detailed characterization of the radiation source, namely the collision debris generated by inelastic collisions at IP8 and propagating along the final focus triplet and the separation dipole, is given. The validation of the model, based on BLM measurements collected during Run 2, is illustrated in Sec. IV. Finally, in Sec. V, the findings for the upcoming Run 3 are reported, quantifying the exposure of the normal-conducting compensator magnets, cold quadrupoles, separation dipole, and recombination dipole in order to assess quench risk and lifetime prospects. A glossary is included at the end of the paper to facilitate the reader with specialized words and acronyms.

II. SIMULATION MODEL: THE LHCb DETECTOR AND THE IR8 LAYOUT

The LHCb detector is designed to perform an indirect search of new physics beyond the Standard Model. For this purpose, the experimental apparatus consists of a single-arm spectrometer optimized to work in the forward direction where the largest b and c quarks production is expected [35]. In order to conduct specific measurements of forward particles, the detector does not provide a 4π coverage of the IP as ATLAS and CMS, but it is spread over 20 m of stacked planar subdetectors placed only on the right-side of IP8 and approaching the vacuum chamber. In order to exploit the space for the detector in the UX85 cavern where the DELPHI experiment had previously been

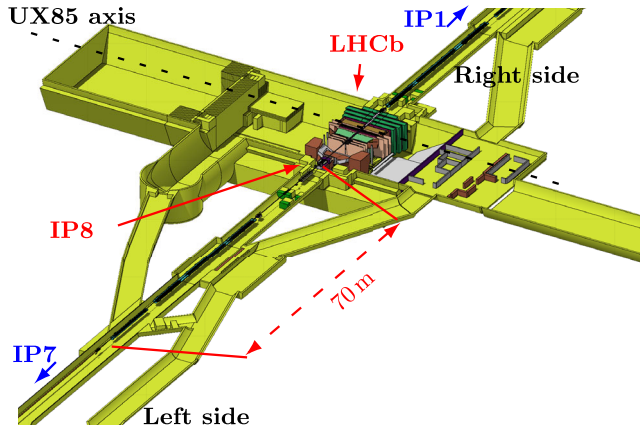

FIG. 1. 3D top view of the FLUKA geometry model of IR8 including the LHCb detector, LHC tunnel, and service areas.

housed, IP8 is displaced by approximately 11 m toward IP7, as shown in Fig. 1. Given the difficulty to perform precise measurements in presence of too many primary vertices, the detector was designed to operate at a lower luminosity than the two general purpose LHC experiments (ATLAS and CMS). The successive upgrades will allow much more data to be handled.

The asymmetry with respect to the IP is a peculiarity of IR8 that makes it unique compared to IR1 and IR5. The shift of IP8 implies that the whole string of the quadrupole triplet and the separation and recombination dipoles is displaced by approximately 11 m toward the left side with respect to the center of the experimental cavern (that is, also the magnetic center of the octant). The shift of IP8 is regained before the dispersion suppressor (DS), resulting in an asymmetric layout of the matching section with respect to IP8.

The LHCb spectrometer induces a horizontal kick of 194 μrad on a 6.5 TeV proton. Depending on its powering, the kick is directed toward the outside or the inside of the ring. This orbit bump is compensated by a system of three normal-conducting dipoles, shown in yellow in the schematic layouts in Fig. 2. The long normal-conducting dipole MBXWH is placed on the left side of IP8, as symmetric counterpart of the LHCb spectrometer giving an opposite kick, which turns out to be identical when considering two protons leaving IP8 in opposite directions. Two short compensators are placed just on the IP side of the (left and right) triplet, producing each a small kick of 49 μrad opposite to the larger one of the MBXWH or spectrometer close by. On the whole, a 6.5 TeV proton traveling from one triplet to the other through IP8 experiences a ± 49, ∓ 194, ± 194, ∓ 49 μrad kick sequence and so arrives in IP8 with an angle of ∓ 145 μrad on the horizontal plane (referred to as spectrometer bump in the text). Since the field intensities of the dipoles are kept constant, this angle

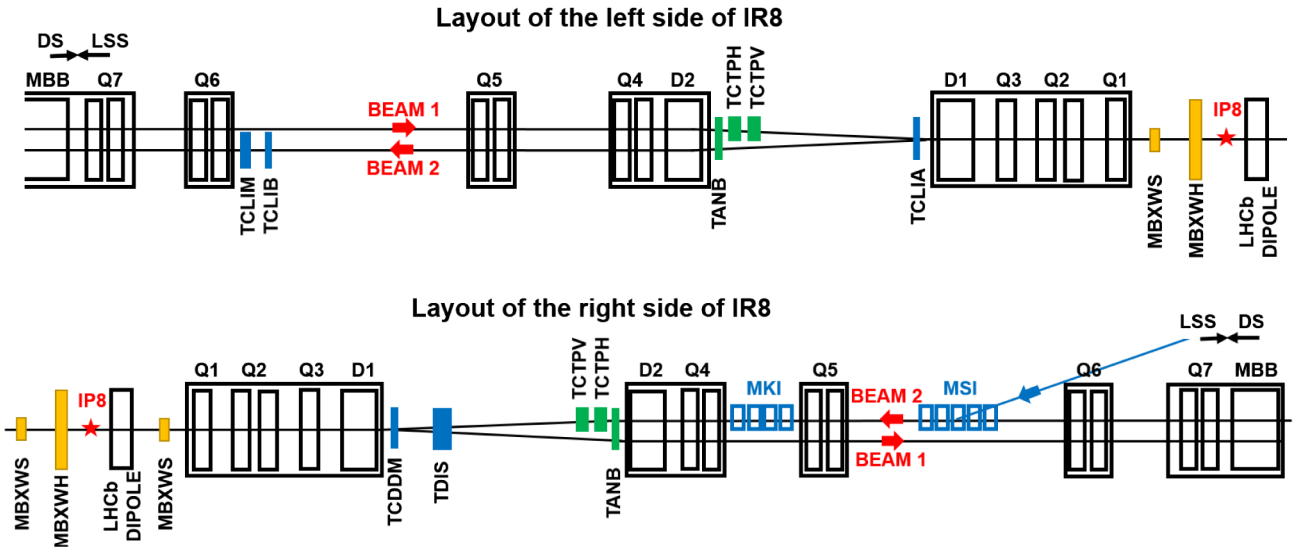

FIG. 2. Schematic layout of both sides of the IR8 Long Straight Section (LSS) in Run 3. The blue elements (magnets and protection absorbers) are related to beam-2 injection. The yellow elements are the normal-conducting compensator magnets (MBXW). The green elements are tertiary collimators and D2 protection absorbers (TANB), as listed in Tables II and III. The element acronyms mean: Q Quadrupoles, D Dipoles, MB Main Bending dipoles (coldmass), TCT Target Collimator Tertiary, TCLI Target Collimator Long Injection protection, TAN Target Absorber Neutral, TCDD Target Collimator for D1 protection, TDIS Target Dump Injection Segmented, MKI Injection Kicker Magnet, MSI Injection Septa Magnet. The central triplet quadrupole Q2 is divided into two identical magnets called Q2A and Q2B in the text hereinafter.

becomes ∓ 135 μrad for $\sqrt{s} = 14$ TeV, as shown in the top trajectory plot in Fig. 3.

The actual angle between the proton momentum in IP8 and the detector axis is determined by the combination of the above bump with the external crossing angle. The latter is required to prevent undesired encounters in the region where the beams share the same vacuum chamber and it is enabled by corrector dipoles [36]. Several configurations with different crossing plane and crossing angle value have been studied and adopted during operation. As an example, at the end of Run 2 in 2018, the external crossing angle was on the horizontal plane. However, for symmetry reasons, the choice of an external crossing angle on the vertical plane is preferred by LHCb, which accumulates equal integrated luminosities with either spectrometer polarity [37]. Therefore, during Run 3, from 2023 onwards, the external crossing angle is planned to be enabled on the vertical plane, resulting in a skew crossing plane in IP8 [38] (see the bottom plot of Fig. 3).

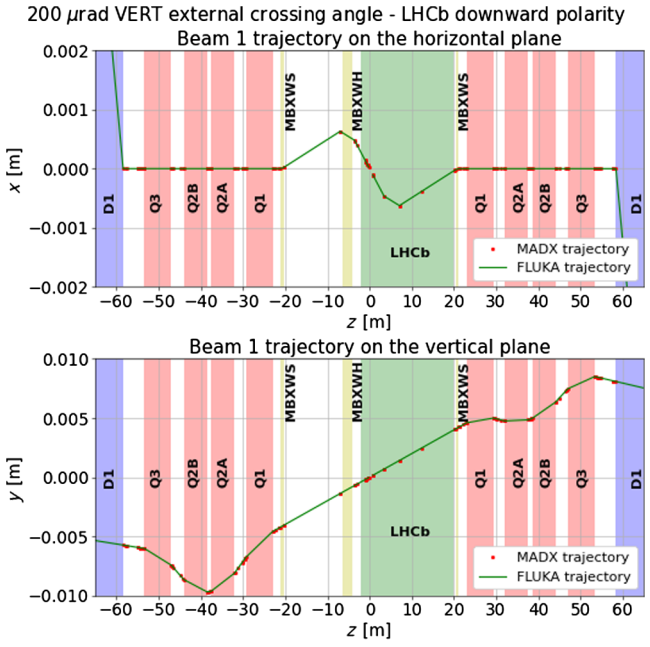

FIG. 3. Beam-1 trajectory between the left and right separation dipole (D1) of IR8, in the horizontal (top) and vertical (bottom) plane, for the reference 7 TeV proton. The green line shows the trajectory calculated with FLUKA and red points are extracted from the optics file generated with MAD-X.

The injection line of the counterclockwise beam (beam 2) joins the LHC on the right side of IR8, implying the presence of septa magnets in the half-cell 6 and kicker

TABLE II. Protection elements on the left side of IP8.

Element	Distance from IP8 (m)	Protection from
TCLIA.4L8	−73	Injected beam B2
TCTPV.4L8	−116	Incoming beam B1
TCTPH.4L8	−118	Incoming beam B1
TANB.4L8[a]	−119	Collision debris
TCLIB.6L8	−217	Injected beam B2
TCLIM.6L8	−223	Injected beam B2

[a]Installed during LS2.

TABLE III. Protection elements on the right side of IP8.

Element	Distance from IP8 [m]	Protection from
TCDDM.4R8	71	Injected beam B2
TDIS.4R8[a]	81	Injected beam B2
TCTPV.4R8	116	Incoming beam B2
TCTPH.4R8	118	Incoming beam B2
TANB.4R8[b]	119	Collision debris

[a]Installed during LS2, replacing TDI.4R8.
[b]Installed during LS2.

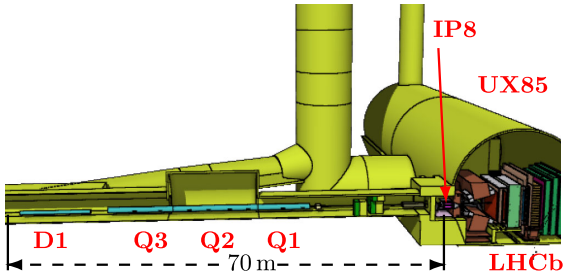

FIG. 4. 3D view (from the inside of the ring) of the FLUKA geometry model including the LHCb experiment and the left side of the LHC with the quadrupole triplet Q1–Q3 and the separation dipole D1.

magnets in the half cell 5, which are switched off during physics production (see Fig. 2). In addition, dedicated injection protection elements are in place, namely, the TCLIA and TCLIB collimators on the left side (see Table II) and the TDI absorber and TCDDM mask on the right side (see Table III). During LS2, the LHC injection protection system was upgraded by the replacement of the TDI with a new segmented absorber, called TDIS [39]. The TDIS protects the downstream elements of LHC (namely the D1 and triplet quadrupole string) during the beam injection phase. It intercepts the injected beam when its orbit deviates from the reference one due to malfunction or failure of the injection kickers. After the beam has been fully injected, the TDIS jaws are opened.

Regarding additional machine protection elements, two tertiary collimators per side (TCTPH and TCTPV) are installed to protect the experiment from the incoming beams (see Fig. 2, Tables II and III). Otherwise, recalling the fact that LHCb was designed to operate at a lower luminosity than ATLAS and CMS, the TAS (target absorber secondaries) and TAN (target absorber neutrals) absorbers and TCL (target collimator long) collimators for physics debris were not necessary in IR8 for Run 1 and Run 2. The TAS is an absorber placed on the IP side of the final focus triplet to protect the first quadrupole (Q1) from the collision debris, while the TAN is an absorber intercepting mostly neutral particles, being placed in front of the recombination dipole (D2) where there is the transition between the common vacuum chamber and the two separate beam pipes. Nevertheless, during LS2, a new TANB (Target Absorber Neutrals at LHCb region) absorber was installed at 120 m from IP8 on both sides, in view of the luminosity increase foreseen for Run 3 [40,41]. On the contrary, the TAS absorber and TCL collimators are still not required in IR8 for the planned operation up to 2×10^{33} cm^{-2} s^{-1}, aiming to produce up to 50 fb^{-1}.

Two FLUKA geometry models of the detector, corresponding to the Run 2 and Run 3 versions, respectively, have been included in the FLUKA repository as developed by the LHCb Collaboration [18]. The Run 3 geometry includes major upgrades in key detector elements, like neutron shielding. Figure 4 gives another 3D view of the comprehensive geometry, with the shafts to the surface. In order to implement this geometry, a Python-based tool for assembling accelerator beam lines (e.g., LHC, SPS, PS) for FLUKA simulations, called Linebuilder, has been used [42]. The software interfaces with a library, the FLUKA Element Database, including the FLUKA geometry models of different accelerator components (magnets, collimators, absorbers, etc.), which are used with a modular approach to build the beam line on the basis of optics (Twiss) files.

At the same time, the BLMs [22,43] are placed according to the positions extracted from the CERN Layout database [44] as well as corrected by visual inspection of the tunnel. Concerning the simulation parameters, the adopted transport thresholds are 1.0 MeV for electrons and positrons and 100 keV for all other particles (except neutrons, transported down to thermal energy). For the benchmarking studies, electromagnetic transport thresholds have been locally decreased to 10 keV in the BLMs, as described in [22]. The beam trajectory over the considered region, as simulated in FLUKA, follows the nominal optics, calculated by means of the MAD-X code, with an accuracy of few μm (see Fig. 3).

III. SOURCE TERM: COLLISION DEBRIS

For proton operation, radiation showers in the experimental IRs are dominated by inelastic nuclear interactions at the IP. Hence, this study does not include elastic interactions, whose products mostly travel with the beam and are possibly intercepted by the collimation system [45]. Each inelastic collision at the IP may generate a large number of secondary particles, on average about 120 with 7 TeV beams. Due to the decay of unstable particles, mainly neutral pions, already 5 mm away from the IP and without interacting with any material, the number of debris particles increases to about 155, of which 50% are photons and 35% are charged pions [45]. While the majority of these particles interacts in the experimental beam pipe and in the detector, the most energetic debris is scattered at small angles with respect to the beam direction. These particles propagate along the beam line in the IRs, impacting the machine elements and determining radiation

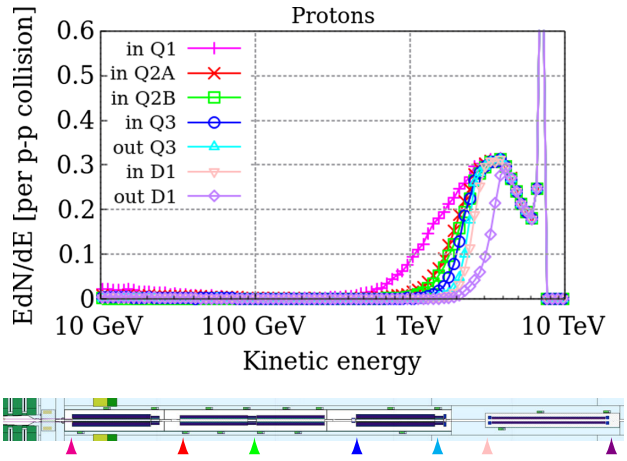

FIG. 5. Energy spectra in lethargy unit, of protons in the vacuum pipe on the right side of IP8 at the position indicated by the triangles in the geometry layout. The colors of the triangles correspond to the locations where the particles are counted (at the entrance and exit of the magnets) and match with the colors of the respective lines in the plot.

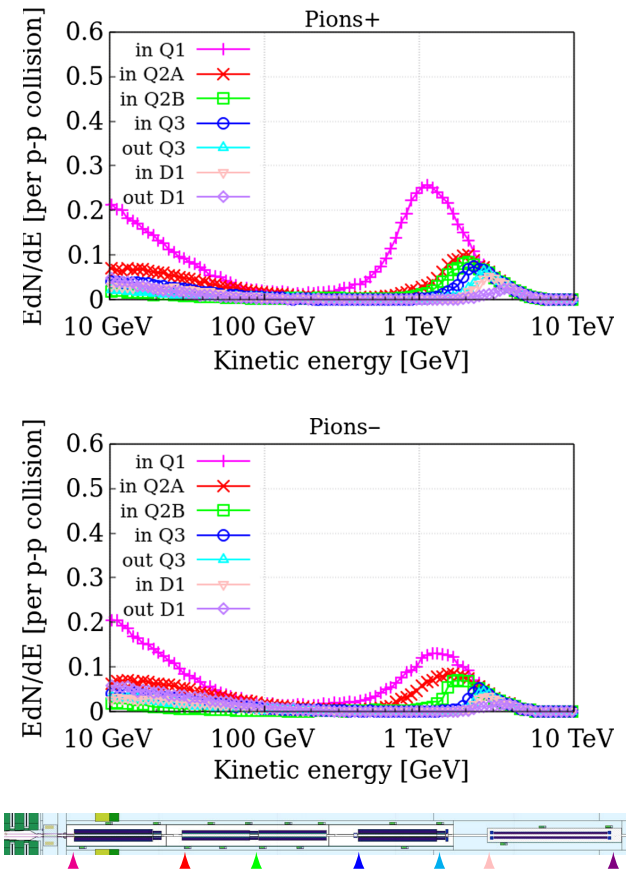

FIG. 6. Energy spectra in lethargy unit, of positive pions (on the top plot) and of negative pions (on the bottom plot) in the vacuum pipe on the right side of IP8 at the position indicated by the triangles in the geometry layout. The colors of the triangles correspond to the locations where the particles are counted (at the entrance and exit of the magnets) and match with the colors of the respective lines in the plot.

levels in the LHC tunnel and in the nearby locations. The power absorbed by the final focus quadrupoles and the separation dipole is mostly due to charged pions that are bent by the magnetic field onto the beam screen walls representing the mechanical aperture. For a luminosity of 4×10^{32} cm^{-2} s^{-1}, this corresponds to 32×10^6 inelastic collisions per second and a power of 33 W toward either (right or left) side.

In this work, the inelastic cross section, including diffractive events, is assumed to be $\sigma_{pp} = 80$ mb [46]. In Figs. 5 and 6, the energy spectra of charged particles travelling inside the vacuum chamber (i.e., protons and charged pions that are the dominant species) are shown at different positions along the triplet and the separation dipole.

Their behavior along the accelerator line is influenced both by the initial conditions of the collision, i.e., the beam crossing scheme and the magnetic fields that they are subject to. As for the triplet, the configuration of the four quadrupoles (Q1, Q2A, Q2B, and Q3) is DFFD (defocusing-focusing-focusing-defocusing) in the horizontal plane for the outgoing beam. The particles with a lower magnetic rigidity than the circulating beam may be captured. As an example, considering the case of $\sqrt{s} = 14$ TeV, only protons with an energy higher than 5.5 TeV can reach up to 200 m from IP8, while a 5 TeV proton is lost before the recombination dipole.

The 7 TeV peak in Fig. 5 is due to diffractive processes, where one interacting proton receives a limited angular kick and is subject to a slight energy loss, this way managing to leave the long straight section (LSS). In the range between 500 GeV and 2 TeV, the fluence at the IP face of the Q1 in IR8 is higher than the values published for IR1 and IR5 [45] due to the absence of the TAS absorber. As already introduced, the TAS absorber, installed in the ATLAS and CMS insertion regions, protects the first triplet quadrupole and considerably reduces the absorbed power as well as the peak dose and power density in its coils. The pion energy spectra of Fig. 6 are peaked at lower energies just above 1 TeV on the Q1 front face, and their average energy increases for larger distances from IP8 as the smaller magnetic rigidity component gets captured along the way. Most pions, especially positively charged, are captured by the magnetic field of the Q1 quadrupole. The pink tail below 100 GeV comes from debris reinteractions in the experimental cavern. As for the high energy part, positive pions are significantly more abundant than negative pions, because a larger fraction of the latter ones does not even reach the triplet due to the combined effect of the crossing angle and the LHCb spectrometer (or MBXWH) field [32,34]. In fact, the top panel of Fig. 7 shows that negative particles are further bent on the same side pointed to by the

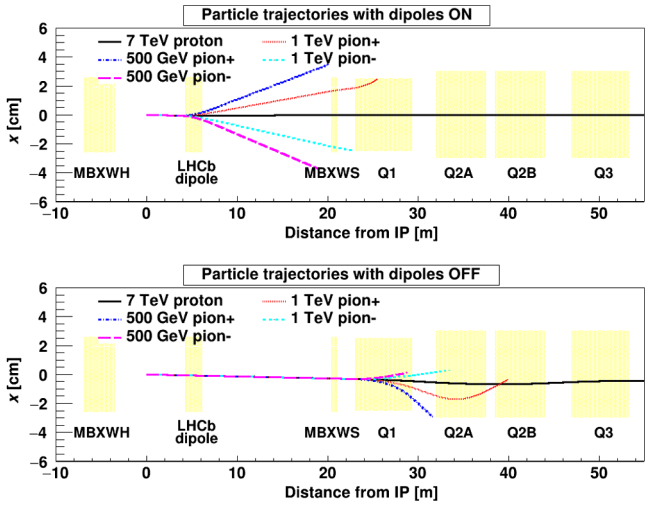

FIG. 7. Beam proton and secondary pion trajectories in the horizontal plane on the right side of IP8, for external crossing in the vertical plane and downward LHCb polarity. Yellow areas indicate the magnet's mechanical aperture. In the bottom panel, the LHCb spectrometer and short compensator fields are academically zeroed, in order to appreciate their effect. The pink, cyan, and red trajectories end where they intercept the beam screen wall in the vertical plane.

crossing angle (at negative x for the considered LHCb polarity) and so miss the Q1 aperture. The role of the LHCb and MBXWH fields is emphasized by the comparison with the bottom panel, where no field is applied before entering the triplet. We note that this difference in the abundance of positive and negative pions is much less dramatic in IR1 and IR5 [45]. The low energy tail of the pink curve in Fig. 6 is not present in the case of IR1 and IR5 due to the shielding provided by the TAS. In addition, reinteractions in the TAS absorber itself cause the peak to be at a lower energy, namely, around 500 GeV and more pronounced than that observed in IR8 [45].

The energy spectra for neutrons and photons traveling inside the vacuum chamber are displayed in Figs. 8 and 9. They are not affected by magnetic fields and propagate in a straight line until they meet an aperture restriction. As shown in Fig. 8, TeV neutrons travel undisturbed beyond the separation dipole, because of their highly forward angular distribution, and are later intercepted by the TANB absorber between the two separate beam tubes. The photon energy spectra in Fig. 9 have a broad peak around a few hundred GeV. As indicated by the difference between the pink and red curves, a sizable quantity of photons is absorbed by the Q1, due to the absence of the TAS. The aperture of the following quadrupoles is larger and so puts the Q2A in the geometrical shadow of the Q1, which ends in the Q2B. Thereby, the latter is also subject to the photon impact, as visualized by the difference between the green and the blue curves.

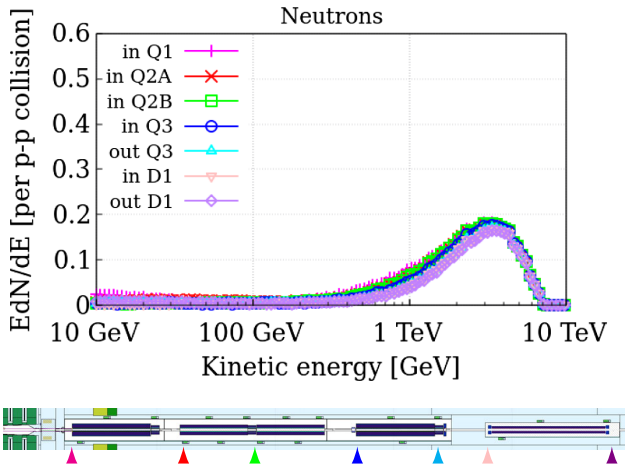

FIG. 8. Energy spectra in lethargy unit, of neutrons in the vacuum pipe on the right side of IP8 at the position indicated by the triangles in the geometry layout. The colors of the triangles correspond to the locations where the particles are counted (at the entrance and exit of the magnets) and match with the colors of the respective lines in the plot.

Considering the spatial evolution of the debris along the triplet and the D1, we find that a crucial role is played by the crossing scheme, coupled with the triplet magnetic configuration. The understanding of this point is also important to work out how possible combinations of different schemes can minimize the coil insulator degradation due to radiation and so increase the magnet lifetime. The power density distribution in the inner layer of the superconducting coils, depending on the polarity of the LHCb spectrometer, is shown in Figs. 10 and 11 for external crossing in the vertical and horizontal plane, respectively.

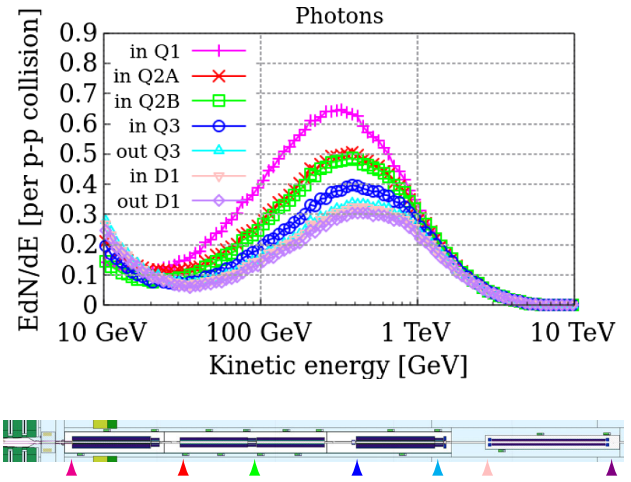

FIG. 9. Energy spectra in lethargy unit, of photons in the vacuum pipe on the right side of IP8 at the position indicated by the triangles in the geometry layout. The colors of the triangles correspond to the locations where the particles are counted (at the entrance and exit of the magnets) and match with the colors of the respective lines in the plot.

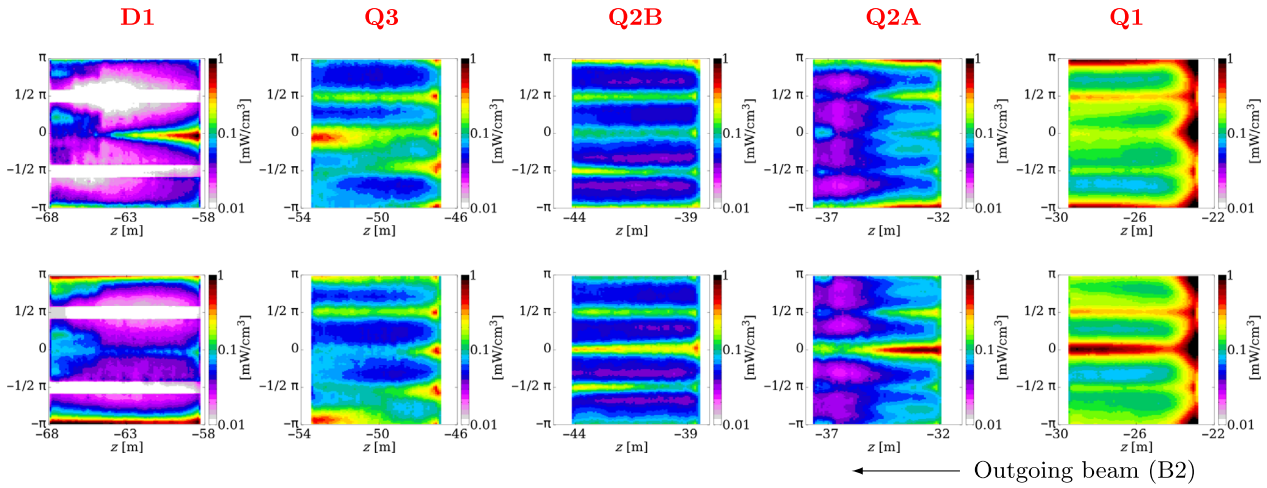

FIG. 10. Color maps of deposited power density as a function of the distance from IP8 (abscissa) and azimuthal angle (ordinate) for the upward (top plots) and downward (bottom plots) polarity of the LHCb spectrometer, with an external half-crossing angle of 200 μrad in the vertical plane. The plots refer, from right to left, to the four quadrupoles Q1-Q2A-Q2B-Q3 and the D1 separation dipole located on the left side of IP8. Power density values are averaged over the radial thickness of their inner coil layer and are given in $\mathrm{mW/cm^3}$, normalized to an instantaneous luminosity of 2×10^{33} $\mathrm{cm^{-2}\,s^{-1}}$, for 7-TeV proton beam operation. The azimuthal angle ϕ runs over the interval $(-\pi, +\pi]$ in radians, where $\phi = 0$ is the horizontal direction pointing outside the ring, $\phi = \pi/2$ is the vertical direction opposite to gravity, and $\phi = \pm\pi$ is the horizontal direction pointing inside the ring.

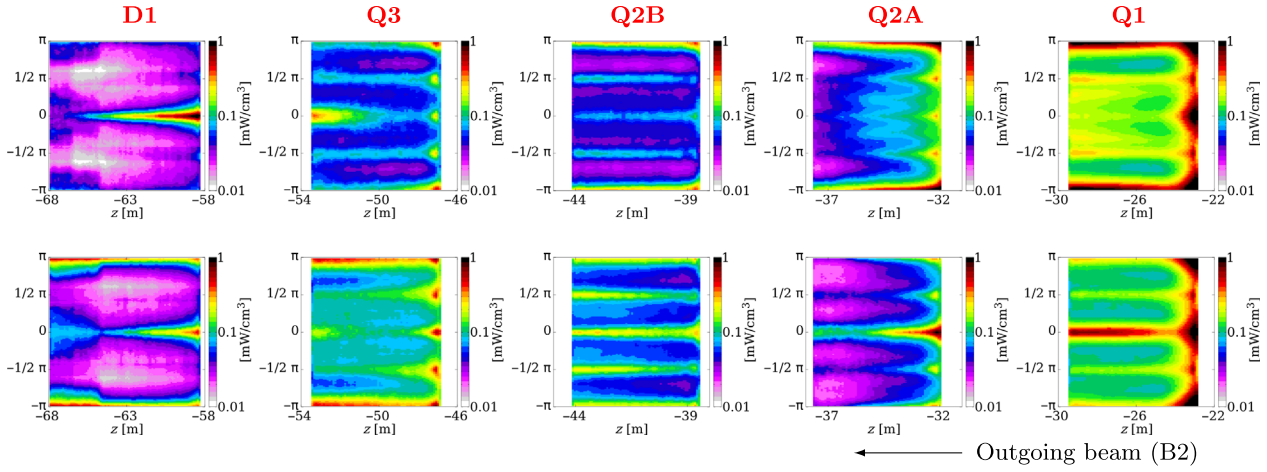

FIG. 11. The same as Fig. 10 with an external half crossing angle of 250 μrad in the horizontal plane.

The debris leaves the IP around the direction of the outgoing beam, as determined by the actual crossing angle. This results from the superposition of the spectrometer bump on the horizontal plane and the external crossing enabled by the orbit corrector magnets. If the external crossing is horizontal (as in Fig. 11), the crossing angle in IP8 sits on the horizontal plane. If the external crossing is vertical (as in Fig. 10), the crossing plane in IP8 is skew. In other words, the latter is never vertical inside the LHCb experiment. The presence of the normal-conducting compensator magnets and the LHCb dipole, acting only in the horizontal plane, causes the charged debris to be intercepted mainly on the horizontal plane, for either external crossing option. The peak power density in the Q1 and first half of the Q2 quadrupole lies on the inside of the ring ($\phi = \pm\pi$) for LHCb upward polarity and on the outside ($\phi = 0$) for LHCb downward polarity. As an effect of the triplet quadrupole field, a reversal of the peak position takes place later, as clearly seen at the non-IP extremity of Q3. In case of external crossing on the vertical plane, another lower peak is found in Q1 at $\phi = \pi/2$. Moreover, for LHCb downward polarity (bottom plots in Fig. 10), the positively charged debris, which is concentrated around $\phi = \pm\pi$ at the D1 entrance, is further pushed by the separation dipole field toward the inside of the ring and this significantly amplifies its impact on the D1 coils, as made apparent afterward in Fig. 14.

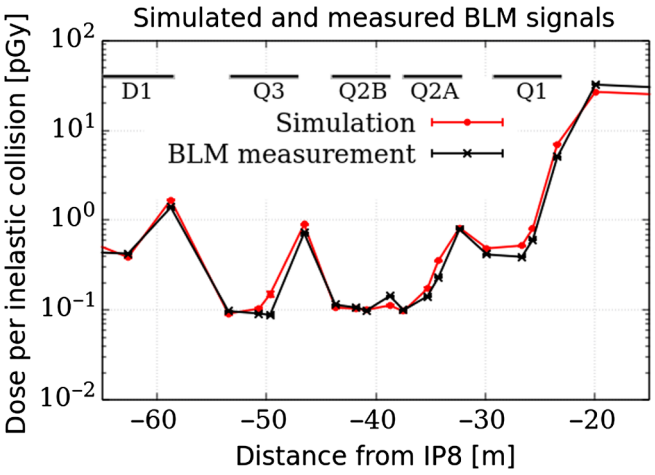

FIG. 12. Simulated (in red) and measured (in black) BLM signals along (from right to left) the four quadrupoles Q1-Q2A-Q2B-Q3 and the D1 separation dipole located on the left side of IP8. All dose values are given per inelastic nuclear interaction generated by 6.5 TeV proton beams colliding in IP8 on the horizontal plane with a half crossing angle of −395 μrad (pointing inside the ring). The experimental data are the result of averaging signals of several fills recorded from August 14, 2018, to October 11, 2018.

IV. RUN 2

A. Beam loss monitor measurements

The BLM system is an essential part of the machine protection architecture to ensure safe LHC operation [43]. The beam losses are monitored in real time through the dose values collected in the BLMs. These are cylindrical ionization chambers featuring parallel aluminum electrode plates filled with nitrogen gas. More than 3600 BLMs are placed around the LHC in selected locations. The signals are converted to dose rate in Gy s^{-1}. The front-end electronics provides 12 output signals (running sums "RS") corresponding to integration periods from 40 μs to 84 s. Beam losses along the accelerator may induce BLM dose rate values exceeding the predefined threshold and so trigger a beam dump request, which is meant to prevent cold magnet quenching or equipment (e.g., collimator) damage. The BLM thresholds are set depending on beam energy and loss duration, in relation to possible hazardous losses originating from the injected or circulating beams. For this study, the BLM signals with the maximum integration time were postprocessed subtracting the noise floor from the measured signals in order to accurately estimate low doses. This technique has been already used in the previous BLM benchmark studies with FLUKA [22].

B. Simulation benchmarking

The simulation has been benchmarked against BLM signals measured during proton physics fills in Run 2. The simulated configuration corresponds to the Run 2 layout with the 2018 6.5 TeV optics. An external horizontal crossing of −250 μrad (with beams pointing inside the ring) was assumed to be coupled to the LHCb spectrometer downward polarity. The latter implies that the incoming beam is further deflected by −145 μrad.

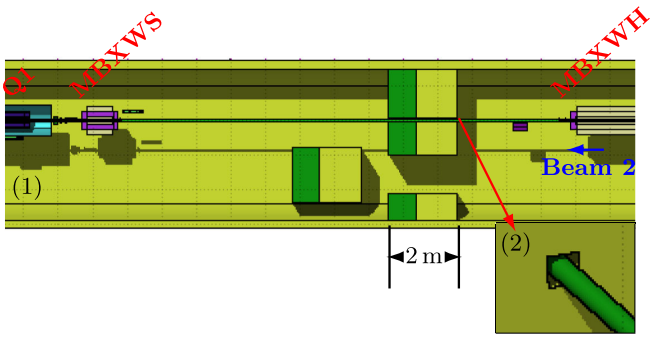

FIG. 13. (1) Top view of the FLUKA geometry model of the left side of IR8 including the shielding between the two normal-conducting dipoles (MBXWH and MBXWS). The shielding consists of transversal walls designed not to block the passage. Each wall is made of a 120-cm thick concrete layer (upstream, in the direction of the outgoing beam, Beam 2) and a 80-cm thick steel layer. (2) 3D plot of the FLUKA geometry model of the aperture of the shielding wall through which the vacuum chamber passes.

Figure 12 presents the comparison between measurements and simulation predictions in terms of dose per 13 TeV center-of-mass inelastic collision. A previous benchmark study focused on the right-side triplet of both LHCb and ATLAS, with regard to Run 1 operation with 4 TeV proton beams [23]. The authors found that simulated signals were on average 20% and 50% higher than data in IR1 and IR8, respectively. The larger overestimation in IR8 was tentatively attributed to secondary particles generated upstream of the Q1 and reaching the BLMs by traveling outside the magnets. The artificial suppression of their contribution in the simulation led to values lower than measurements. In reality, some of these particles are intercepted by external material not included in the simulation model. In this work, special care was devoted to refine the FLUKA geometry, especially on the left side, where the aperture of the shielding wall between the two normal-conducting dipoles (MBXWH and MBXWS, as shown in Fig. 13) turned out to play a crucial role to our benchmarking purposes. Assuming a square hole of 12-cm edge in the aforementioned shielding around the beam pipe, the resulting agreement is on average within 20%, compatibly with systematic uncertainties. This represents a significant improvement with respect to the 50% average discrepancy found in the previous study, especially for the Q2 and Q3 BLMs.

V. RUN 3: PREDICTIONS FOR THE UPCOMING HIGH LUMINOSITY ERA

An important outcome of this study is the review of the impact of the Upgrade I of LHCb on the accelerator

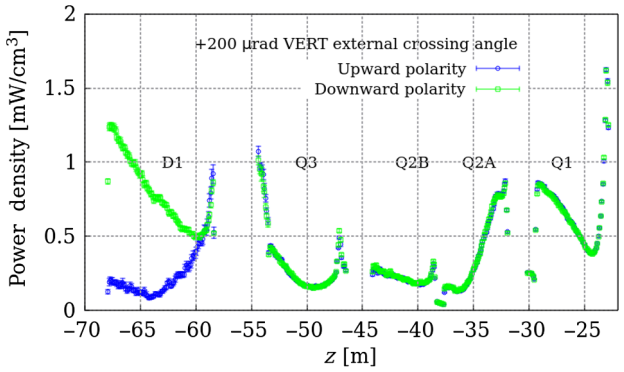

FIG. 14. Longitudinal profile of peak power density in the superconducting coils along the triplet and the D1 (from right to left) on the left side of IP8 (at $z = 0$). Values are averaged over the cable radial thickness and normalized to an instantaneous luminosity of 2×10^{33} cm^{-2} s^{-1} (representing the Run 3 target). The azimuthal resolution is of 2°. External vertical crossing has been simulated for $\sqrt{s} = 14$ TeV in combination with either upward (blue points) or downward (green points) polarity of the LHCb spectrometer.

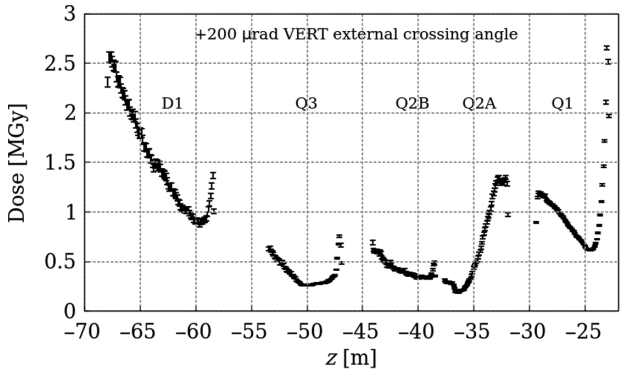

FIG. 15. Longitudinal profile of peak dose in the superconducting coils along the triplet and the D1 (from right to left) on the left side of IP8 (at $z = 0$). The azimuthal and radial resolution is of 2° and 3 mm, respectively. Values refer to the external vertical crossing and an integrated luminosity of 24 fb^{-1}, half of which was collected with either polarity of the LHCb spectrometer at $\sqrt{s} = 13.6$ TeV.

elements in IR8. During 2022, the first year of Run 3, the external crossing at IP8 will be in the horizontal plane, with an integrated luminosity forecast of 4 fb^{-1}[1] at 6.8 TeV proton beam energy. Then, from 2023 to 2025, the external crossing shall be switched to the vertical plane, aiming to record an additional 24 fb^{-1}. So most of the planned integrated luminosity will be produced in the latter scenario, which we simulated with a +200 μrad half angle, implying a vertical momentum component toward the top. This was applied to 7-TeV[2] beams and combined with (i) a +135 μrad kick for the upward polarity of the LHCb spectrometer, giving in IP8 a half crossing angle of ≃240 μrad on a skew half plane oriented at $\phi = 56°$ (see the caption of Fig. 10 for the azimuthal angle definition), as defined in the FLUKA manual [19]; (ii) a −135 μrad kick for the downward polarity of the LHCb spectrometer, giving in IP8 the same half crossing angle of ≃240 μrad on a skew half plane oriented at $\phi = 124°$.

A. The triplet and separation dipole

The first aspect to assess is the operational margin with respect to the magnet quench limit. To do so, one has to evaluate the maximum power density deposited in the superconducting coils, which in steady-state conditions is usually calculated by averaging over the cable transverse area. Figure 14 shows the peak power density profile along the triplet and the D1 dipole on the left side of IP8, for the two polarities of the LHCb spectrometer. Both configurations display an absolute maximum at the IP side of Q1, due to the absence of the TAS. For the Run 3 instantaneous luminosity of 2×10^{33} cm^{-2} s^{-1}, its value is less than one-half of the design limit. In fact, the quench limit for the triplet was estimated to be 1.6 mW/g, namely, 13 mW/cm^3, and a safety factor of 3 was taken in defining the design limit at 4.3 mW/cm^3 [27]. Nevertheless, our result confirms that a Q1 protection strategy is required in view of the Upgrade II of LHCb, as the instantaneous luminosity further increases by a factor of 7.5, driving the Q1 peak very close to the quench limit and well beyond the values already reached in the IR1 and IR5 triplets with a luminosity doubling the ATLAS and CMS design value. Looking at the debris behavior shown in Fig. 10, one can see that the peaks are located in the horizontal plane, on opposite sides for the two spectrometer polarities. The peak profile is the same up to the D1 IP face, where the trend changes. There, in the configuration corresponding to the downward polarity, the dominant component of the debris, positively charged, is concentrated toward the inside of the ring, as a result of its passage through the magnetic field of the triplet. As the separation dipole deflects positive particles into the ring, debris losses rise along the magnet up to reaching 1.25 mW/cm^3 at the non-IP end of the D1. Like for the Q1, this is not alarming for Run 3 but should be addressed in view of Upgrade II.

The other important aspect to be studied is material degradation due to the radiation exposure. In particular, the long-term deterioration of the coil insulator, as a function of the radiation dose accumulated with the integrated luminosity, can jeopardize the magnet functionality and so determines its lifetime. Figure 15 shows the peak dose profile that is expected to be produced during the last 3 years of Run 3, assuming external crossing in the vertical plane and an equal sharing of the integrated luminosity target between the two LHCb polarity configurations. The 2D dose map for the three highest peaks is displayed in

[1]The actual luminosity delivered in 2022 has been 1fb^{-1} .
[2]At the time of these studies, the actual Run 3 beam energy was not yet defined.

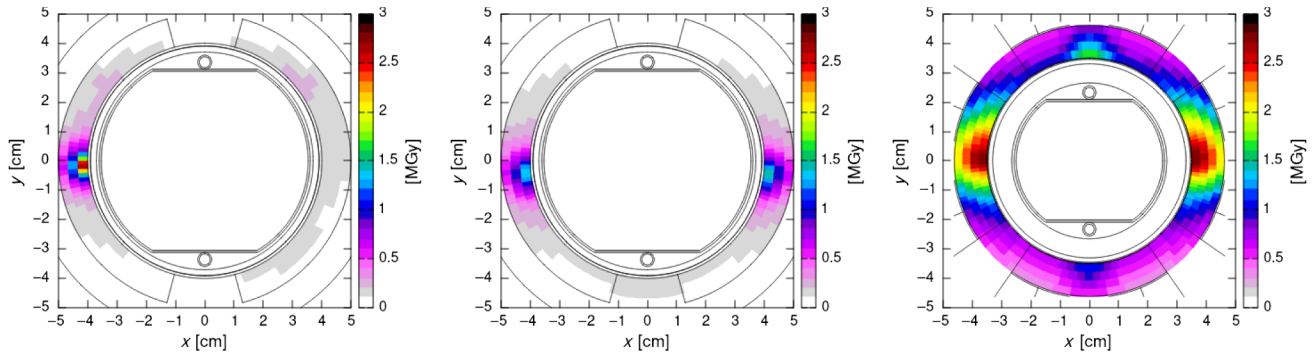

FIG. 16. Transverse dose distribution on the D1 non-IP face (left), D1 IP face (center), and Q1 IP face (right) for external crossing in the vertical plane (with +200 μrad half angle). The contribution of both 2023 to 2025 operation (24 fb^{-1} at $\sqrt{s} = 13.6$ TeV) and Run 1 is included, assuming that half of the respective integrated luminosity is produced with either LHCb polarity. Plots refer to the magnets on the left side of IP8 (at $z = 0$).

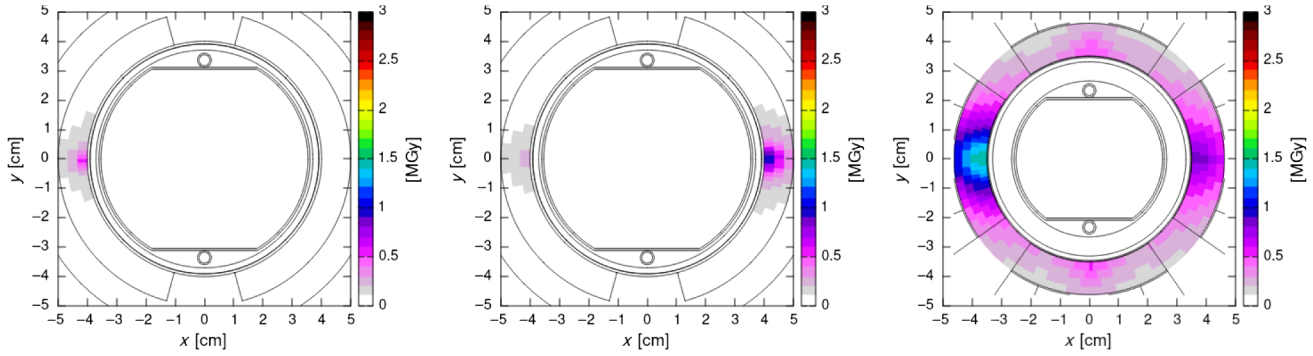

FIG. 17. Transverse dose distribution on the D1 non-IP face (left), D1 IP face (center), and Q1 IP face (right) for external crossing in the horizontal plane. The contribution of both 2022 operation (4 fb^{-1} at $\sqrt{s} = 13.6$ TeV) and Run 2 (6.6 fb^{-1} at $\sqrt{s} = 13$ TeV from 2015 to 2018) is included, assuming that half of the respective integrated luminosity is produced with either LHCb polarity. Plots refer to the magnets on the left side of IP8 (at $z = 0$).

Fig. 16, after adding the Run 1 contribution. On the other hand, Fig. 17 reports the picture for external crossing in the horizontal plane, as adopted during Run 2 and planned for 2022.

In total, the maximum dose predicted on the IP face of Q1 by the end of Run 3 in 2025 is 4.5 MGy on the left of IP8, rising to about 6 MGy on the right of IP8, where the triplet is more exposed. As far as D1 is concerned, the maximum dose is 3 MGy on the non-IP face and 2.5 MGy on the IP face. These numbers are safely below the damage limit of 30 MGy that is known to apply to Q1–Q3 [47]. Nonetheless, their increase for the ultimate LHCb Upgrade II target of 400 fb^{-1} requires a dedicated analysis, specifically on the corrector magnets embedded in the triplet, whose multiwire cable insulation may start to degrade already over a dose range not exceeding 10 MGy.

B. The compensator magnets

As discussed in Sec. II, the normal-conducting magnets compensating for the LHC spectrometer kick are the closest elements to IP8. The one most impacted by the collision debris is the short compensator on the right side, absorbing 13.5 W at the Run 3 instantaneous luminosity. Despite its larger mass, the long compensator MBXWH, that is, well shielded by a concrete wall that seals off the experimental cavern on the left side, gets only 11 W. In fact, thanks to its proximity to IP8, it is also missed by the most energetic particles that travel at too low angles with respect to the longitudinal axis. A weak point is represented by the coils on the magnet IP face, especially for the short compensator on the right side. The peak dose reached just above the vacuum pipe (assuming external vertical crossing with +200 μrad half angle) is predicted to surpass 10 MGy by the end of Run 3. These findings suggest implementing before the end of Run 3 a suitable tungsten piece acting as coil protection, in order to reduce the maximum dose by a factor of few, also in view of the further luminosity increase later envisaged. A minor gain may come from the polarity inversion of the external crossing angle.

C. The recombination dipole

The first HL-LHC object installed in the machine during LS2 was the TANB, a tungsten absorber earlier mentioned in Sec. II. It was designed to shield the D2 recombination

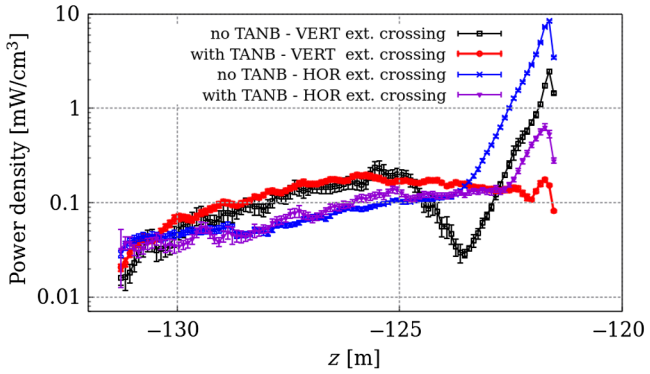

FIG. 18. Longitudinal profile of peak power density in the D2 superconducting coils on the left side of IP8 (at $z = 0$). Values are averaged over the cable radial thickness and normalized to an instantaneous luminosity of 2×10^{33} cm^{-2} s^{-1} (representing the Run 3 target). The azimuthal resolution is of 2°. Four cases have been simulated for $\sqrt{s} = 14$ TeV and downward LHCb polarity: external crossing in the horizontal or vertical plane, with or without the TANB.

dipole on both sides of IP8 from forward high-energy neutral particles produced by proton-proton collisions. As a result, the total power absorbed by the D2 cold mass at 2×10^{33} cm^{-2} s^{-1} decreases from 30 W [33] to 6 W (less on the right side of IP8, because of the additional protection provided by the TCDDM mask). Moreover, Fig. 18 shows the TANB effect on the peak power density in the D2 superconducting coils. The maximum on the IP face is reduced by more than a factor of 10 for both external crossing schemes. This translates into a maximum dose to the coil insulator lower than 1 MGy by the end of Run 3 (2025), after an additional 28 fb^{-1} at $\sqrt{s} = 13.6$ TeV. Thanks to its proximity to the recombination dipole, the TANB may also fulfill its protection functions in the Upgrade II scenario, as current studies confirm.

VI. CONCLUSIONS AND OUTLOOK

In this paper, we have evaluated radiation levels induced by proton beam collisions in the LHCb detector. The FLUKA model of IR8 has been improved and further validated by comparing the BLM dose values measured in 2018 physics fills with the simulation predictions in the region of the triplet and separation dipole. The obtained good agreement corroborates the FLUKA model reliability for addressing the challenges raised by the future luminosity increase. In particular, we used the model to review the implications of running LHCb at 2×10^{33} cm^{-2} s^{-1}, as planned in the upcoming Run 3 of the LHC. The collision debris from proton operation at that instantaneous luminosity, about 5 times higher than in Run 2, is predicted not to pose any threat with respect to quench limits and cryocapacity. On the other hand, after accumulating an additional 28 fb^{-1} by the end of 2025, a maximum dose of about 6 MGy is expected to be reached in the Q1 coils on the right of IP8. The most exposed high-order correctors embedded in the triplet would get 2–3 MGy. In parallel, the front coils of the short normal-conducting compensators would reach 10–12 MGy. The installation of tungsten shields appears to be a viable mitigation solution, although dedicated studies are needed to properly design them. Finally, the recombination dipole benefits from the TANB effective protection.

The investigation of the Upgrade II scenario is currently ongoing, aiming to indicate effective solutions that allow accelerator operation at 1.5×10^{34} cm^{-2} s^{-1} and for 400 fb^{-1} in LHCb. This calls for the comprehensive study of several measures. Some of them naturally follow the conclusions of this work, such as the shielding of the short compensators, the Q1 quadrupoles and D1 separation dipoles, and the TANB cooling. Other required work is the construction of a new wall in the UX85 cavern [48] and the possible integration of physics debris collimators (TCL) in the machine around LHCb.

ACKNOWLEDGMENTS

Research supported by the HL-LHC project and by the HL-LHC-UK project. We thank Riccardo De Maria and Stephane Fartoukh for providing us with optics input as well as François Butin, Francisco Sanchez Galan, and Maud Wehrle for making available relevant information as well as the technical drawings that were crucial for the geometry description development. We also wish to acknowledge the support of the LHCb Collaboration, who kindly shared the FLUKA model of the LHCb detector.

APPENDIX: GLOSSARY

D1: Separation Dipole. The D1 dipole is placed in the experimental IR just downstream of the triplet magnets with respect to the outgoing beam direction and it has a single cold bore for both LHC beams. Together with the recombination dipole, it brings the beams to collide at the IP [1,49].

D2: Recombination Dipole. The D2 dipole is placed in the experimental IR just upstream of the matching section with respect to the outgoing beam direction. It has two separate vacuum chambers slightly closer to each other than in the LHC arc. Together with the separation dipole, it brings the beams to collide at the IP [1,49].

DS: Dispersion Suppressor. The DS is the transition region between the LHC arc and the LSS. It is designed to reduce the machine dispersion inside the IR [1,49].

HL-LHC and *HiLumi*: High-Luminosity LHC. HL-LHC is the upgrade of the LHC accelerator which aims to fully exploit the physics potential of the LHC, starting from the LHC Run 4. The nominal (ultimate) HiLumi target is to reach a leveled luminosity of $5(7.5) \times 10^{34}$ cm^{-2} s^{-1} and an integrated luminosity of 3000 (4000) fb^{-1} [1,49].

IP: Interaction Point. The IP is the point where the two LHC beams cross over. For the ATLAS, CMS, and ALICE

insertion, the IP (IP1, IP5, and IP2, respectively) corresponds to the middle of the LSS and the octant. Only for the LHCb insertion, as described in the text, the IP (IP8) is not placed in the center of the octant [1,49].

IR: Insertion Region. An insertion region is a part of the LHC between the dispersion suppressors of two neighboring arcs. Four insertion regions, called experimental insertion regions, host one of the four main LHC experiments: the ATLAS detector is placed in IR1, the ALICE detector in IR2, the CMS detector in IR5, and the LHCb detector in IR8. Moving from the arc to the IP, the experimental IR includes a matching section (MS), a recombination dipole (D2), a separation dipole (D1), and a triplet assembly (also called final focus triplet). The other four insertion regions have a specific role in the operation of LHC: IR3 and IR7 host the momentum and betatron collimation system, respectively, IR4 hosts the accelerating cavities and IR6 hosts the extraction system leading to the beam dump [1,49].

LHC: Large Hadron Collider. Its circumference is approximately 27 km and it is divided into octants. Each octant hosts a straight region (called in the text insertion region) surrounded by two arcs [1,49].

LS: Long Shutdown. For example, the LS2 (from 2019 to mid 2022) is the Shutdown period after the Run 2 operation of the LHC. An updated long-term schedule of the LHC operation is published [15].

LSS: Long Straight Section. It is the quasistraight section between the dispersion suppressors of the IR [1,49].

MS: Matching Section. It consists of a string of quadrupole magnets located between the DS and the final focus triplet [1,49].

Upgrade I of LHCb: The Phase-I Upgrade of LHCb carried out during LS2, aiming to collect 50 fb^{-1} in Run 3–4.

Upgrade II of LHCb: The proposed Phase-II Upgrade of LHCb planned for LS4, aiming to collect 300 fb^{-1} in Run 5–6.

[1] O. Aberle *et al.*, High-Luminosity Large Hadron Collider (HL-LHC): Technical design report, *CERN Yellow Reports: Monographs* (2020), 10.23731/CYRM-2020-0010.

[2] Werner Herr and B. Muratori, Concept of luminosity, in *Proceedings of CERN Accelerator School, Zeuthen* (Report No. CERN-2006-002).

[3] ATLAS Collaboration, ATLAS: Technical proposal for a general-purpose pp experiment at the Large Hadron Collider at CERN, LHC technical proposal, CERN, Geneva, Report No. CERN-LHCC-94-43, 1994.

[4] CMS Collaboration, CMS, the Compact Muon Solenoid: Technical proposal, LHC technical proposal, CERN, Geneva, Report No. CERN-LHCC-94-38, CERN-LHCC-P-1, 1994.

[5] LHCb Collaboration, LHCb: Technical Proposal, CERN, Geneva, Report No. CERN-LHCC-98-04, 1998.

[6] LHCb Collaboration, Framework TDR for the LHCb Upgrade: Technical Design Report, Technical Report No. CERN-LHCC-2012-007, LHCb-TDR-12, 2012.

[7] LHCb Collaboration, Measurement of *CP*-Averaged Observables in the $B^0 \to K^{*0}\mu^+\mu^-$ Decay, Phys. Rev. Lett. **125**, 011802 (2020).

[8] LHCb Collaboration, Test of lepton universality in beauty-quark decays, Nat. Phys. **18**, 277 (2022).

[9] ATLAS, CMS, and LHCb Collaborations, Combination of the ATLAS, CMS and LHCb results on the $B^0_{(s)} \to \mu^+\mu^-$ decays, CERN, Geneva, Technical Report No. LHCb-CONF-2020-002, ATLAS-CONF-2020-049, CMS PAS BPH-20-003, 2020.

[10] LHCb Collaboration, Physics case for an LHCb Upgrade II-Opportunities in flavour physics, and beyond, in the HL-LHC era, CERN, Geneva, Technical Report No. LHCB-PUB-2018-009, CERN-LHCC-2018-027, LHCC-G-171, 2018.

[11] LHCb Collaboration, Framework TDR for the LHCb Upgrade II-Opportunities in flavour physics, and beyond, in the HL-LHC era, CERN, Geneva, Technical Report No. CERN-LHCC-2021-012, LHCB-TDR-023, 2021.

[12] LHCb Collaboration, LHCb operations plots webpage, https://lbgroups.cern.ch/online/OperationsPlots/index.htm [accessed 2022].

[13] ATLAS Collaboration, ATLAS experiment-public results, https://twiki.cern.ch/twiki/bin/view/AtlasPublic/LuminosityPublicResultsRun2#Multiple_Year_Collision_Plots [accessed 2022].

[14] CMS Collaboration, CMS luminosity-public results, https://twiki.cern.ch/twiki/bin/view/CMSPublic/LumiPublicResults#LHC_and_CMS_luminosity_records [accessed 2022].

[15] CERN, Longer term LHC schedule, http://lhc-commissioning.web.cern.ch/schedule/LHC-long-term.htm [accessed: 2022].

[16] CERN, LHC/HL-LHC plan (last update February 2022), https://hilumilhc.web.cern.ch/sites/default/files/HL-LHC_Janvier2022.pdf [accessed 2022].

[17] G. Arduini, O. Bruning, M. Lamont, and R. Tomas, HL-LHC luminosity ramp-up (at the start of the fill and over years), in *Proceedings of 171st HiLumi WP2 Meeting*, http://lhc-commissioning.web.cern.ch/schedule/LHC-long-term.htm.

[18] M. Karacson, Evaluation of the radiation environment of the LHCb Experiment, CERN-THESIS-2016-246, Ph.D. thesis, 2016.

[19] CERN, Fluka website, https://fluka.cern.

[20] C. Ahdida, D. Bozzato, D. Calzolari, F. Cerutti, N. Charitonidis, A. Cimmino *et al.*, New capabilities of the FLUKA multi-purpose code, Front. Phys. **9**, 788253 (2022).

[21] G. Battistoni, T. Boehlen, F. Cerutti, P. W. Chin, L. S. Esposito, A. Fassò *et al.*, Overview of the FLUKA code, Ann. Nucl. Energy **82**, 10 (2015).

[22] A. Lechner, B. Auchmann, T. Baer, C. Bahamonde Castro, R. Bruce, F. Cerutti *et al.*, Validation of energy deposition simulations for proton and heavy ion losses in the CERN Large Hadron Collider, Phys. Rev. Accel. Beams **22**, 071003 (2019).

[23] A. Lechner, Particle interactions with matter, CERN Yellow Rep. School Proc. **5**, 47 (2018).

[24] A. Mereghetti, Performance evaluation of the SPS scraping system in view of the High Luminosity LHC, CERN-THESIS-2015-116, Ph.D. thesis, 2015.

[25] N. V. Mokhov and F. Cerutti, Beam-material interaction, CERN Yellow Report No. CERN-2016-002, p. 83 (2016).

[26] N. V. Mokhov, I. L. Rakhno, I. S. Tropin, F. Cerutti, L. S. Esposito, and A. Lechner, Energy deposition studies for the High-Luminosity Large Hadron Collider inner triplet magnets, Phys. Rev. ST Accel. Beams **18**, 051001 (2015).

[27] N. V. Mokhov, I. L. Rakhno, J. S. Kerby, and J. B. Strait (CERN-US LHC Construction Collaboration), Protecting LHC IP1/IP5 Components Against Radiation Resulting from Colliding Beam Interactions, CERN, Geneva, Technical Report No. FERMILAB-FN-0732, CERN-LHC-Project-Report-633, 2003.

[28] M. Sabaté-Gilarte and F. Cerutti, Energy deposition study of the CERN HL-LHC optics v1.5 in the ATLAS and CMS insertions, in *Proceedings of the 12th International Particle Accelerator Conference, IPAC-2021, Campinas, SP, Brazil* (JACoW, Geneva, Switzerland, 2021), pp. 76–79.

[29] A. Tsinganis and F. Cerutti, Impact of collision debris in the HL-LHC ATLAS and CMS insertions, in *Proceedings of IPAC-2017, Copenhagen, Denmark* (JACoW, Geneva, Switzerland, 2017), TUPVA021, 10.18429/JACoW-IPAC2017-TUPVA021.

[30] M. Calviani, Updated FLUKA simulations for P8 in support of R2E activities (UX85, US85 and UW85), CERN, Geneva, Technical Report No. 1099674 v.1.6, 2011.

[31] R. B. Appleby and A. Mereghetti, The FLUKA model of IR8, CERN, Geneva, Technical Report No. LHC-Project-Note-427, CERN-LHC-Project-Note-427, 2010).

[32] F. Cerutti, HL-LHC - FLUKA simulation: Radiation challenges for the machine, in *5th Workshop on LHCb Upgrade II*, https://indico.cern.ch/event/897697/.

[33] L. S. Esposito, F. Cerutti, A. Lechner, A. Mereghetti, V. Vlachoudis, and A. Patapenka, Power load from collision debris on the LHC point 8 insertion magnets implied by the LHCb luminosity increase, Conf. Proc. **C130512**, 1382 (2013), https://cds.cern.ch/record/1636136/files/CERN-ACC-2013-0285.pdf.

[34] I. Efthymiopoulos, G. Arduini, V. Baglin, H. Burkhardt, F. Cerutti, S. Claudet *et al.*, LHCb upgrades and operation at 10^{34} cm^{-2} s^{-1} luminosity–a first study, CERN, Geneva, Technical Report No. CERN-ACC-NOTE-2018-0038, 2018.

[35] LHCb Collaboration, The LHCb Detector at the LHC, J. Instrum. **3**, S08005 (2008), also published by CERN Geneva in 2010.

[36] W. Herr, M. Meddahi, and Y. Papaphilippou, How do we have to operate the LHCb spectrometer magnet?, CERN, Geneva, Technical Report No. LHC-Project-Note-419, 2008.

[37] J. Albrecht, M. J. Charles, L. Dufour, M. D. Needham, C. Parkes, G. Passaleva *et al.*, Luminosity scenarios for LHCb Upgrade II, CERN, Geneva, Technical Report No. LHCb-PUB-2019-001, 2019.

[38] S. Fartoukh, S. Kostoglou, M. Solfaroli Camillocci, G. Arduini, H. Bartosik, C. Bracco *et al.*, LHC configuration and operational scenario for Run 3, CERN, Geneva, Technical Report No. CERN-ACC-2021-0007, 2021.

[39] J. A. Uythoven, N. Biancacci, C. Bracco, L. Gentini, B. Goddard, A. Lechner *et al.*, Injection protection upgrade for the HL-LHC, in *Proceedings of the 6th International Particle Accelerator Conference, IPAC-2015, Richmond, VA* (JACoW, Geneva, Switzerland, 2015), pp. 2136–2139.

[40] F. Sanchez Galan, TANB-functional specification, CERN, Geneva, Technical Reports No. 1960537 v.1.0, No. LHC-TANB-ES-0002 v.1.0, 2018.

[41] H. Garcia Gavela, F. Sanchez Galan, and M. Santos, TANB (neutral beam absorber) in A4R8 AND A4L8, CERN, Geneva, Technical Report No. 1961576 v.1.0, LHC-TANB-ES-0003 v.1.0, 2018.

[42] A. Mereghetti, V. Boccone, F. Cerutti, R. Versaci, and V. Vlachoudis, The FLUKA LineBuilder and Element DataBase: Tools for building complex models of accelerator beam lines, in *Proceedings of the 3rd International Conference on Particle Accelerator Conference, IPAC-2012, New Orleans, LA, 2012* (IEEE, Piscataway, NJ, 2012), https://accelconf.web.cern.ch/IPAC2012/papers/WEPPD071.pdf; [Conf. Proc. **C1205201**, 2687 (2012)].

[43] E. B. Holzer, B. Dehning, E. Effnger, J. Emery, V. Grishin, C. Hajdu *et al.*, Beam loss monitoring for LHC machine protection, Phys. Procedia **37**, 2055 (2012).

[44] CERN, CERN Layout Database, https://layout.cern.ch/ [accessed 2021].

[45] M. Brugger, F. Cerutti, and L. S. Esposito, The environmental challenges: Impact of radiation on machine components, Adv. Ser. Dir. High Energy Phys. **24**, 177 (2015).

[46] ATLAS Collaboration, Measurement of the Inelastic Proton-Proton Cross Section at $\sqrt{s} = 13$ TeV with the ATLAS Detector at the LHC, Phys. Rev. Lett. **117**, 182002 (2016).

[47] M. Tavlet, A. Fontaine, and H. Schonbacher, Compilation of radiation damage test data, CERN, Geneva, Technical Report No. 98-01, 1998.

[48] F. Butin *et al.*, A shielding wall in UX85 for LHC Run 5, CERN, Geneva, Technical Report No. 2424228 v.0.1, 2021.

[49] L. Evans, The Large Hadron Collider, Annu. Rev. Nucl. Part. Sci. **61**, 435 (2011).